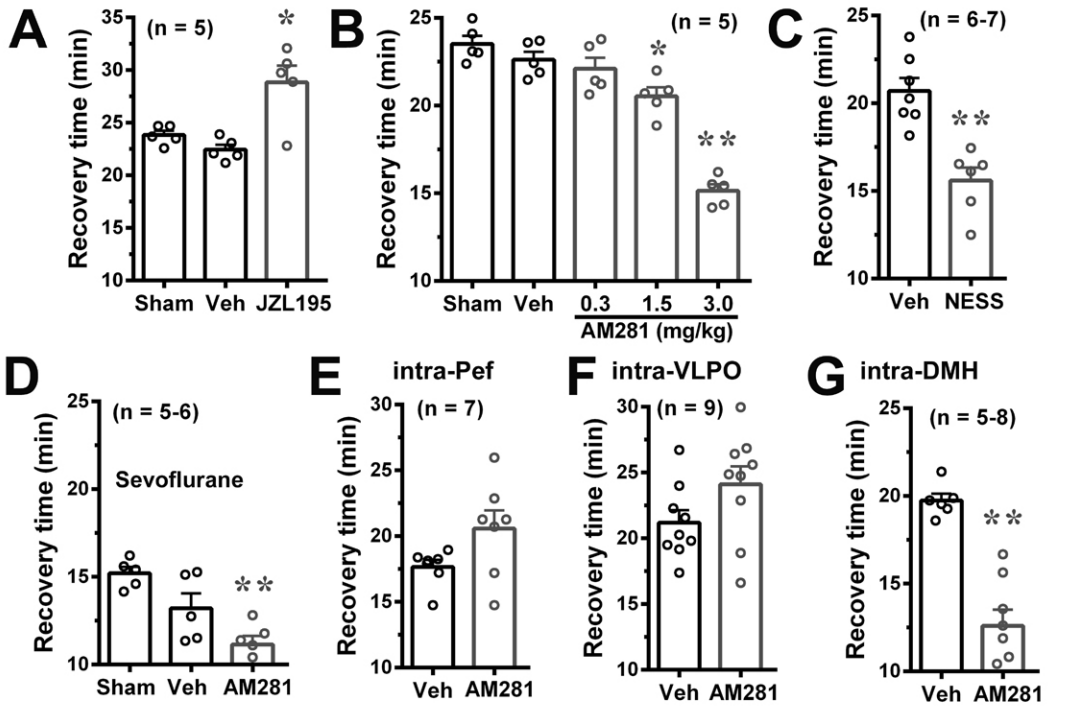

Figure 1 eCB modulation of arousal from anesthesia. (**A**, **B**) Relative to sham anesthesia (Sham), JZL195 (A: 20 mg/kg, i.p.) and AM281 (B: 0.3, 1.5, 3.0 mg/kg, i.p.), but not vehicle (Veh), respectively prolongs and shortens recovery time after isoflurane anesthesia. (**C**) Relative to Veh, NESS0327 (NESS, 0.3 mg/kg, i.p.) significantly shortens recovery time after isoflurane anesthesia. (**D**) Relative to Sham, AM281 (3 mg/kg, i.p.) but not Veh significantly shortens recovery time after sevoflurane anesthesia. (**E**, **F**) Neither intra-Pef (E) nor intra-VLPO microinjection (F) of AM281 (0.1 μg/0.3 μl/side) significantly affects recovery time (E: $p = 0.0723$ F: $p = 0.231$) after isoflurane anesthesia. (**G**) Bilateral intra-DMH microinjection of AM281 (0.1 μg/0.3 μl/side) significantly shortens recovery time after isoflurane anesthesia. All summary graphs show means ± SEMs; n = numbers of rats in each group. * $p<0.05$ and ** $p<0.01$ vs. Sham or Veh, Tukey's *post-hoc* test after one-way ANOVA (A: $F_{2,12} = 11.63$, $p<0.05$; B: $F_{4,20} = 46.17$, $p<0.01$; D: $F_{2,13} = 12.13$, $p<0.01$) or Student *t* test (C, E-G)

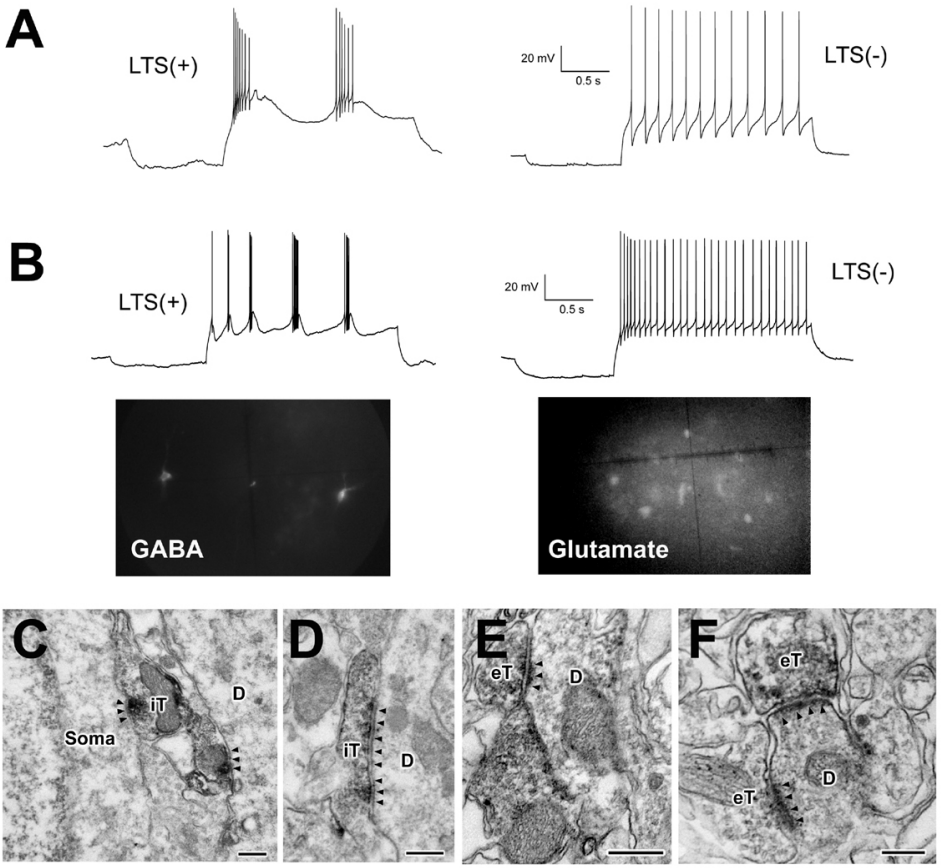

Figure 2 Electrophysiologicalc and ultra-structural characteristics of DMH GABAergic and glutamatergic neurons. (**A**) Sample current clamp traces (> 20 repetitions) show two distinct types of DMH neurons with or without low-threshold spikes, i.e., LTS(+) or LTS(-), respectively, elicited when the membrane is depolarized from negative potentials. (**B**) Sample current clamp traces (> 20 repetitions) of LTS(+) or LTS(-) (top) are recorded from fluorescent DMH neurons (bottom photos) of GABAergic (GABA) and glutamatergic neurons (Glutamate) from GAD67-GFP and vGlut2-iCreERT2 mutant mice, respectively. (**C**-**F**) Electron microscopic images (3 mice) show CB_1R-immunoreactive peroxidase reaction product in DMH GABAergic axonal terminals (iT in C and D) or glutamatergic axonal terminals (eT in E and F). Black arrowheads identify symmetric and asymmetric synaptic contacts of the presumed GABAergic and glutamatergic nature, respectively, with the neuronal soma profile (Soma) or dendritic profile (D). Scale bar = 0.25 μm.

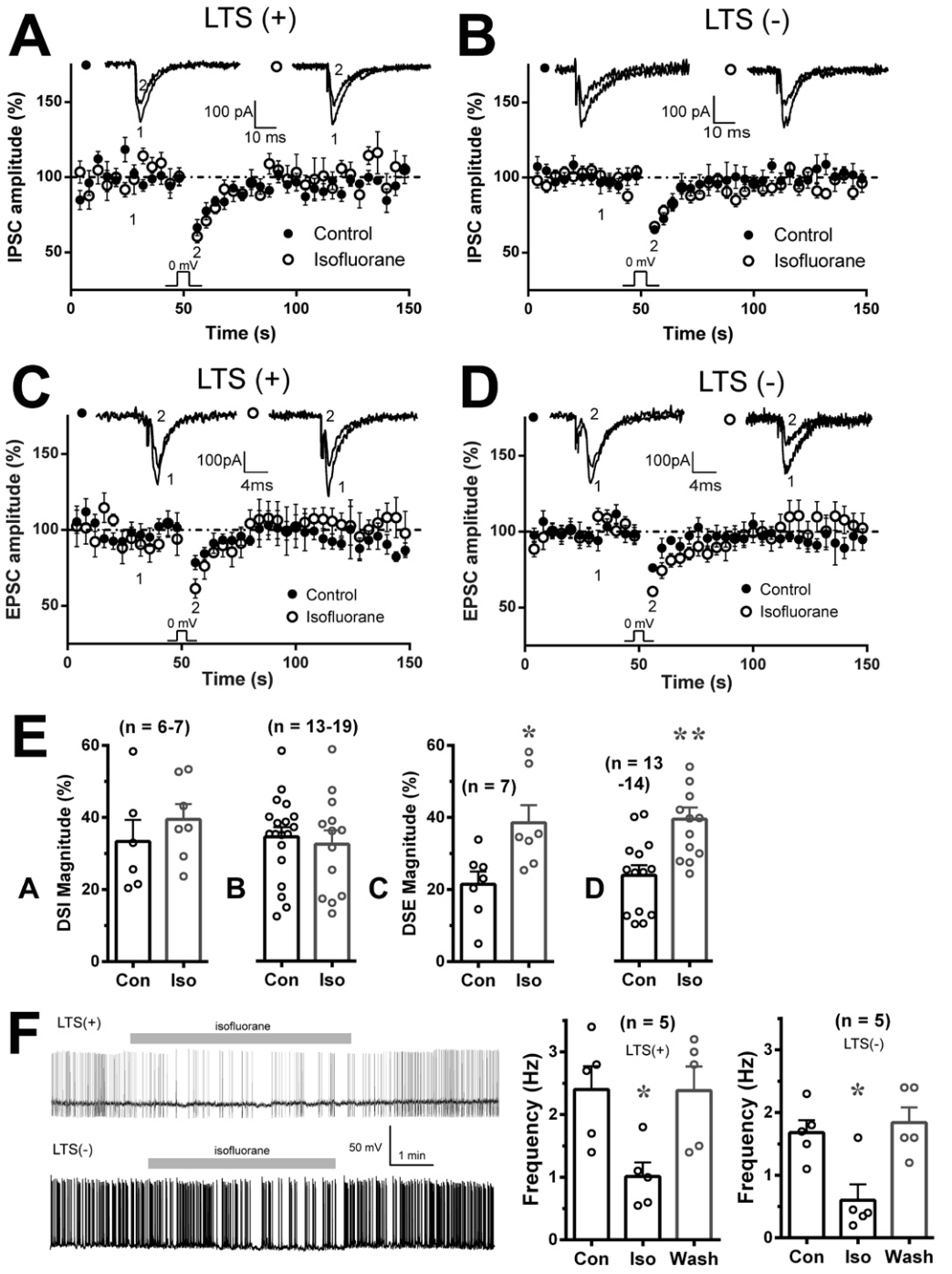

Figure 3 Isoflurane increase of eCB signaling in DMH glutamatergic but not GABAergic synapses. **(A-E)** Plots of normalized IPSC (A, B) or EPSC amplitude (C, D) and summary histograms (E) show that DSI magnitude of DMH LTS(+) and LTS(-) neurons does not significantly change following bath application of isoflurane (Iso) as compared to baseline (Con) (E: A, $p = 0.1333$; B, $p = 0.8729$), which, however, significantly increases DSE magnitude of both LTS(+) and LTS(-) neurons. Representative IPSC and EPSC traces are superimposed on the top of each plot. The summarized data in E is the first time point after depolarization of the cell, which is marked with "2" in A-D. **(F)** The representative traces (left) and summary histograms (right) show that relative to baseline (Con), bath application of isoflurane (Iso) induces rapid hyper-polarization of the membrane potential and significantly decreases of the firing rate of both LTS(+) and LTS(-) neurons in the DMH, which return to the baseline levels after washout (Wash). All summary graphs show means ± SEMs; n = numbers of rats recorded in each group. * $p < 0.05$ and ** $p < 0.01$ vs. Con, Student *t* test (E) or Tukey's *post-hoc* test after one-way ANOVA (F: LTS(+), $F_{2,12} = 5.669$, $p < 0.05$; LTS(-), $F_{2,3212} = 8.517$, $p < 0.01$).

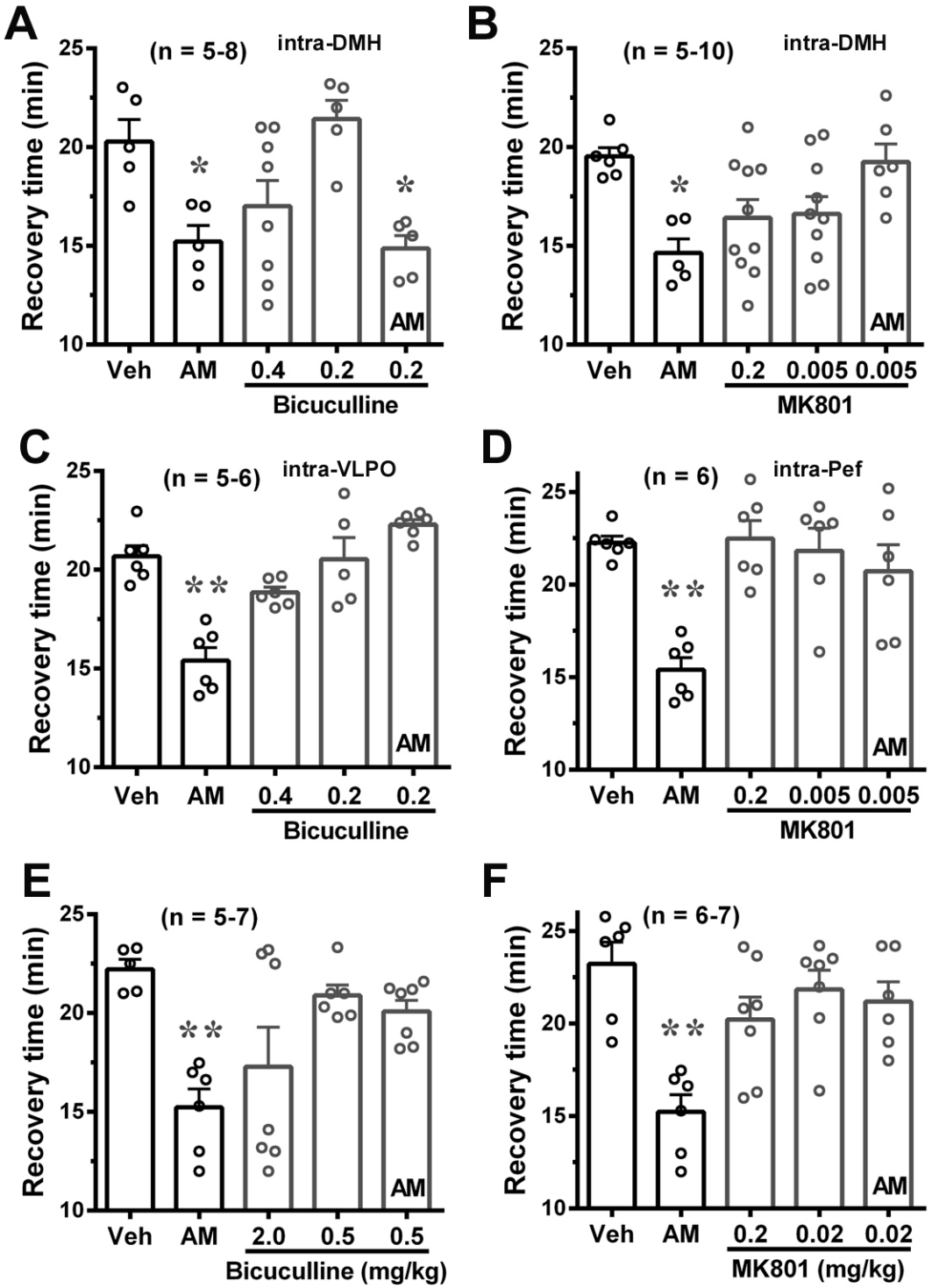

Figure 4 Blockade of CB_1R at DMH glutamatergic synapses accelerates arousal through VLPO and Pef. Both high and low doses of the GABAR antagonist bicuculline and the NMDAR antagonist MK801 are used in order to reveal their dose-response effects on arousal after anesthesia. **(A-D)** Relative to vehicle (Veh), AM281 (AM, 3.0 mg/kg, i.p.) significantly shortens recovery time, which is not significantly affected by bilateral intra-DMH microinjection of bicuculline (A: 0.2 μg/side/injection). Bilateral intra-DMH microinjection of MK801 (B: 0.005 μg/side/injection), intra-VLPO microinjection of bicuculline (E: 0.2 μg/side/injection), and intra-Pef microinjection of MK801 (D: 0.005 μg/side/injection), which do not significantly affect recovery time on their own, prevent AM281 (3 mg/kg, i.p.) from shortening recovery time. **(E, F)** Relative to Veh, AM significantly shortens recovery time, which is blocked by an i.p injection of 0.5 mg/kg bicuculline (E) or 0.02 mg/kg MK801 (F) that does not significantly affect recovery time by its own. All summary graphs show means ± SEMs; n = numbers of rats in each group. * $p < 0.05$ and ** $p < 0.01$ vs. Veh, Tukey's *post-hoc* test after one-way ANOVA (A: $F_{4,23} = 22.6$, $p < 0.01$; B: $F_{4,32} = 29.101$, $p < 0.01$; C: $F_{4,24} = 32.101$, $p < 0.01$; D: $F_{4,25} = 15.025$, $p < 0.01$; E: $F_{4,26} = 34.053$, $p < 0.01$; F: $F_{4,27} = 19.273$, $p < 0.01$).

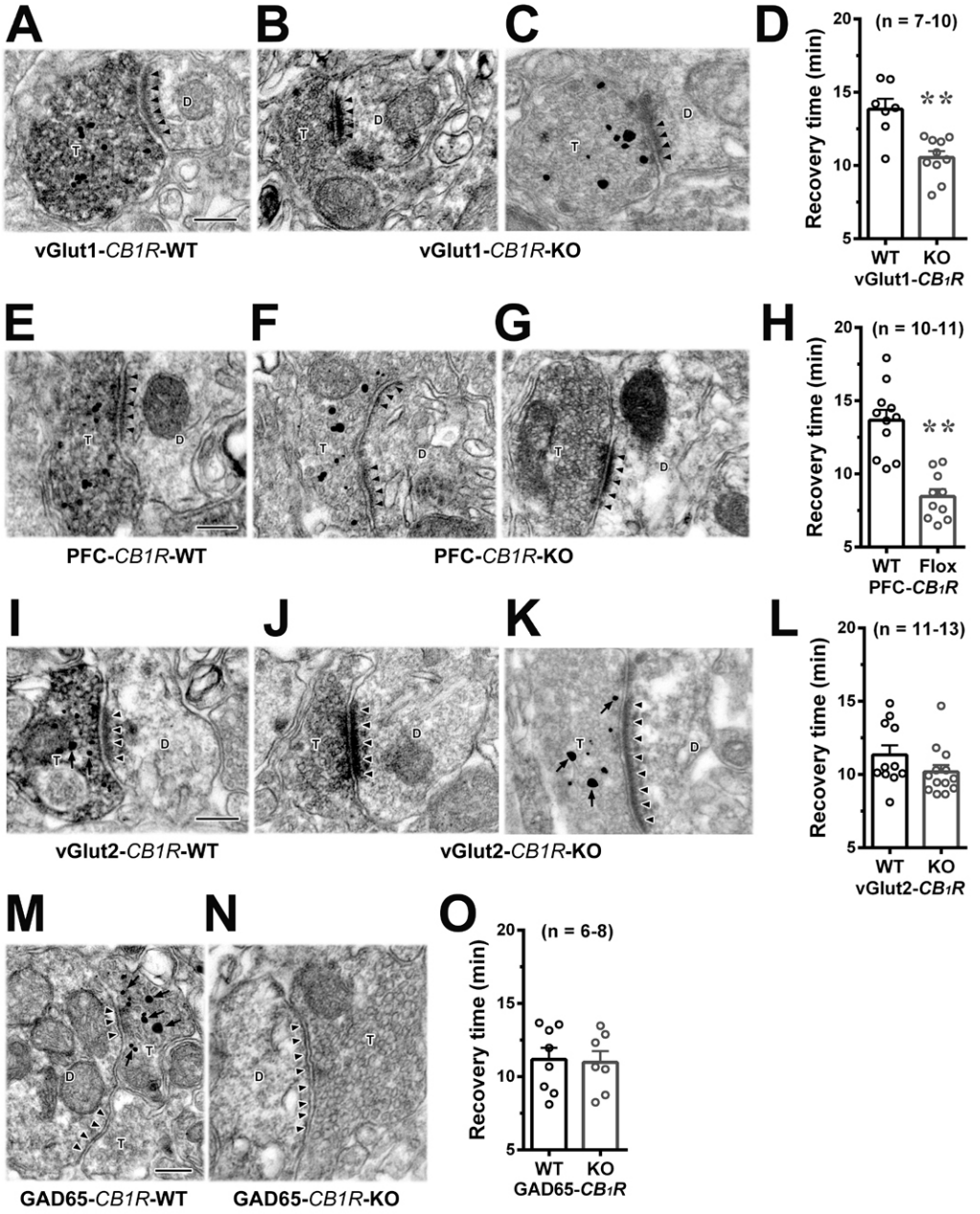

Figure 5 CB_1R deletion from PFC glutamatergic neurons accelerates arousal. (**A-C, E-G, I-K, M, N**) In these electron microscopic images (3-4 mice in each genotype), the presumed glutamatergic and GABAergic nature of an axon terminal (T) is established by the presence of asymmetric (A-C, E-G, I-K) or symmetric (M, N) synaptic contact (black arrowheads) with a dendritic profile (D). CB_1R-immunoreactive (CB_1R-ir) silver grains are in both vGlut1-ir glutamatergic terminals in the DMH of vGlut1-*CB_1R*-WT mice (A) or PFC-*CB_1R*-WT mice (E) or the Pef of vGlut2-*CB_1R*-WT mice (I) and vGlut1-immunonegative (vGlut1-in) (C, G) or vGlut2-in (K) glutamatergic terminals in the DMH of vGlut1-*CB_1R*-KO mice (C) or PFC-*CB_1R*-KO mice (G) or the Pef of vGlut2-*CB_1R*-KO mice (K) but not in vGlut1-ir (B, F) or vGlut2-ir (J) glutamatergic terminals in the DMH of vGlut1-*CB_1R*-KO mice (B) or PFC-*CB_1R*-KO mice (F) or the Pef of vGlut2-*CB_1R*-KO mice (J). Similarly, CB_1R-ir silver grains are in GABAergic terminals in the DMH of GAD65-*CB_1R*-WT mice (M) but not in GAD65-*CB_1R*-KO mice (N). Scale bar = 0.25 μm. (**D, H, L, O**) A significant decrease of recovery time is present in vGlut1-*CB_1R*-KO (D) and PFC-*CB_1R*-KO mice (H), but not vGlut2-*CB_1R*-KO (L: p=0.151) and GAD65-*CB_1R*-KO mice (N: p=0.8659), relative to corresponding wild-type littermates (WT). All summary graphs show means ± SEMs; n = numbers of mice in each group. * p<0.05 and ** p< 0.01 vs. WT, Student t test

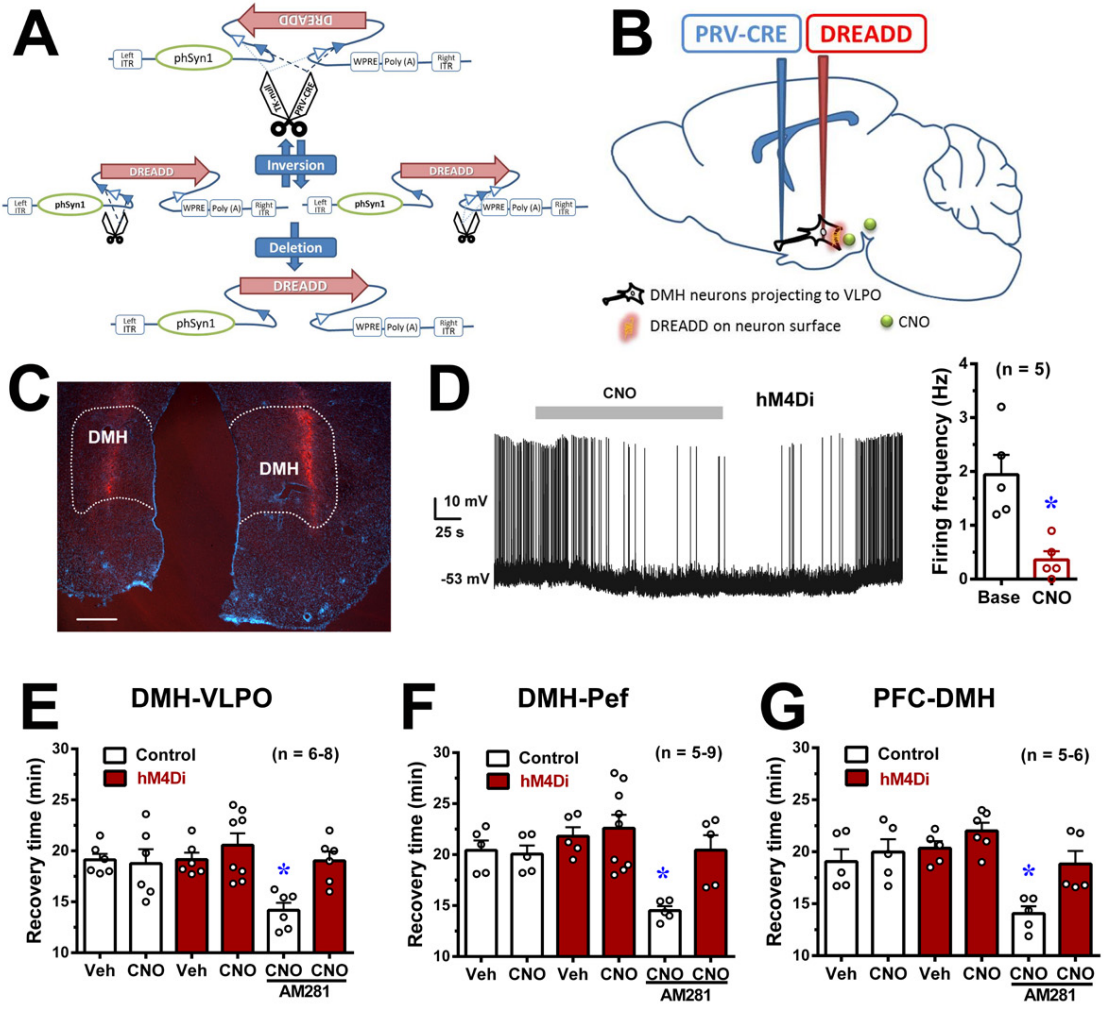

Figure 6 PFC-DMH-Pef/VLPO inactivation counteracts AM281 effects on arousal. (A) The AAV-DREADD-mCherry employs the FLEX Switch strategy utilizing 2 pairs of heterotypic, antiparallel loxP-type recombination sites to achieve Cre-mediated transgene inversion and expression. L-ITR, left-inverted terminal repeat; R-ITR, right-inverted terminal repeat; phSyn1, promoter of human synapsin I; WPRE, woodchuck hepatitis posttranscriptional regulatory element; Poly (A), polyadenylic acid tail. (B) An illustration of intra-VLPO and intra-DMH injection of PRV-Cre and DREADD, respectively, and CNO activation of DREADD. (C Coronal brain section shows red mCherry fluorescence in bilateral DMH after intra-DMH and intra-VLPO injection of DREADD and PRV-Cre, respectively. Scale bar = 500μm. (D) The representative trace (left) and summary histogram (right) show that bath application of CNO induces rapid hyper-polarization of the membrane potential and decreases the firing rate in red fluorescence-labeled DMH neurons after intra-VLPO and intra-DMH injection of PRV-Cre and AAV-hM4Di-mCherry, respectively. (E-G) Rats receive an i.p. injection of vehicle (Veh) or CNO with or without AM281 injection (3 mg/kg, i.p.) at 1-2 weeks after receiving both intra-DMH (E, F) or intra-PFC (G) injection of AAV-mCherry (Control) or AAV-hM4Di-mCherry (hM4Di) and intra-VLPO (E), intra-Pef (F) or intra-DMH (G) injection of PRV-Cre. The Control rats receiving both CNO and AM281 show a significant decrease of recovery time ($p<0.05$ or $p<0.01$) than each of other 5 groups (E-G). All summary graphs show means ± SEMs; n = numbers of rats in each group. * $p<0.05$ and ** $p<0.01$ vs. Base or Veh group, Student *t* test (D) or Tukey's *post-hoc* test after one-way ANOVA (E: $F_{5,32} = 4.929$, $p<0.01$; F: $F_{5,28} = 5.767$, $p<0.01$; G: $F_{5,25} = 7.485$, $p<0.01$).

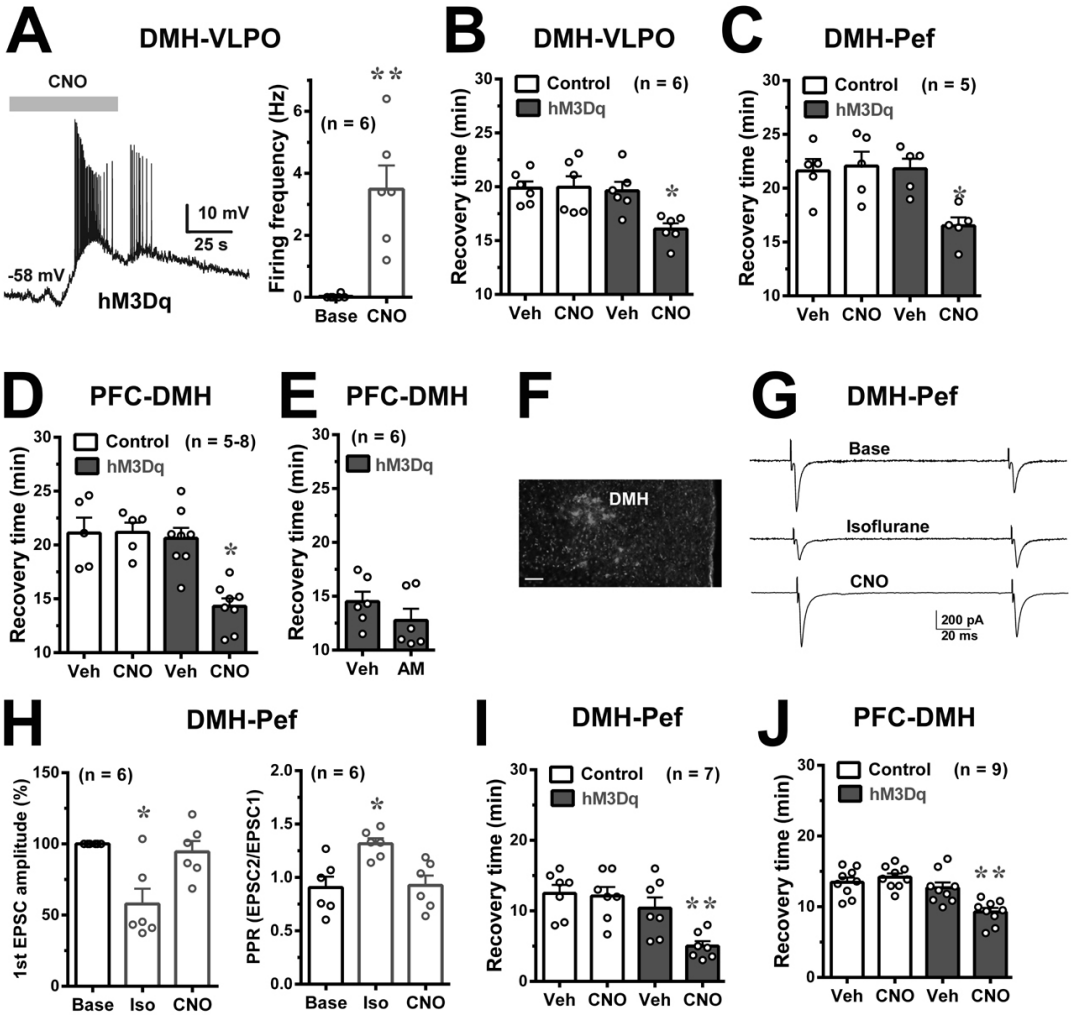

Figure 7 PFC-DMH-Pef/VLPO activation enhances arousal. (A) A sample trace and summary histogram show that CNO induces rapid depolarization of membrane potential and increases firing rate of DMH neurons with red mCherry fluorescence after intra-VLPO and intra-DMH injection of PRV-Cre and AAV-hM3Dq-mCherry (hM3Dq), respectively. (**B-E, I, J**) Rats (B-E), vGlut2-iCreERT2 mice (I) or vGlut1-iCreERT2 mice (J) receive an i.p. (B-E) or intra-Pef (I) or intra-DMH injection (J) of vehicle (Veh) or CNO at 1-2 weeks after receiving intra-DMH (B, C) or intra-PFC (D, E, I, J) injection of AAV-mCherry (Control) or AAV-hM3Dq-mCherry (hM3Dq) with or without intra-VLPO (B), intra-Pef (C) or intra-DMH (D, E) injection of PRV-Cre. The hM3Dq animals receiving CNO show a significant decrease of recovery time ($p<0.05$ or $p<0.01$) than each of other 3 groups (B-D, I, J), but the hM3Dq animals injected with AM281 (AM; 3 mg/kg, i.p.) or its vehicle do not show significant difference ($p = 0.3601$) in recovery time (E). (**F-H**) After intra-DMH injection of hM3Dq into vGlut2-iCreERT2 mice, the DMH neurons containing both vGlut2-driven iCre and the mCherry are visible as red (E: scale bar = 100μm). Sample traces (G) and summary histograms (H) show that with patch clamp recording of Pef neurons and stimulation of DMH input axons, isoflurane reduces and increases the first EPSC amplitude and PPR, respectively, which are reversed by CNO. All summary graphs show means ± SEMs; n = numbers of animals in each group. * $p<0.05$ and ** $p<0.01$ vs. baseline (Base) or Veh, Student *t* test (A, E) or Tukey's *post-hoc* test after one-way ANOVA (B: $F_{3,20} = 5.8893$, $p<0.01$; C: $F_{3,16} = 6.328$, $p<0.01$; D: $F_{3,22} = 12.65$, $p<0.01$; H: left, $F_{2,15} = 9.045$, $p<0.01$; right, $F_{2,15} = 7.492$, $p<0.01$; I: $F_{3,16} = 8.044$, $p<0.01$; J: $F_{3,32} = 11.77$, $p<0.01$).

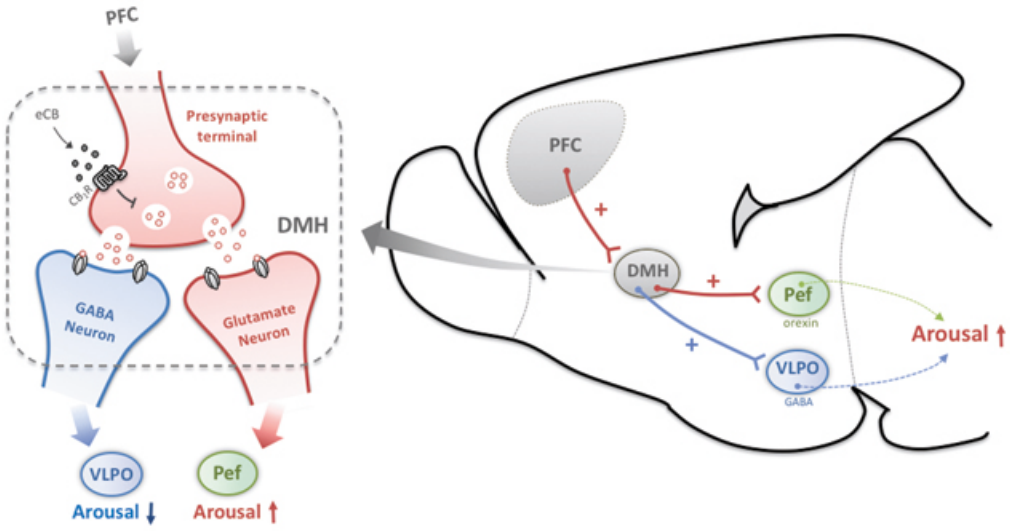

Figure 8 Proposed model for eCB modulation of brain circuitry participating in arousal from anesthesia. Glutamatergic neurons in the prelimbic and infralimbic areas of the PFC directly innervate both glutamatergic and GABAergic neurons in the DMH, which then send glutamatergic axons into the Pef and GABAergic axons into the VLPO, respectively. Glutamatergic DMH-Pef projection innervates excitatory orexin-containing neurons in the Pef, activation of which accelerates arousal. In contrast, GABAergic DMH-VLPO projection innervates inhibitory GABA-containing neurons in the VLPO, activation of which suppresses arousal. Thus, reduced eCB activation of CB_1R in axon terminals of glutamatergic PFC-DMH projection increases presynaptic release of glutamate, which activates inhibitory DMH-VLPO projection, excitatory DMH-Pef projection or both. Then, suppression of the inhibitory VLPO neurons, enhancement of the excitatory Pef neurons, or both accelerate arousal after anesthesia.

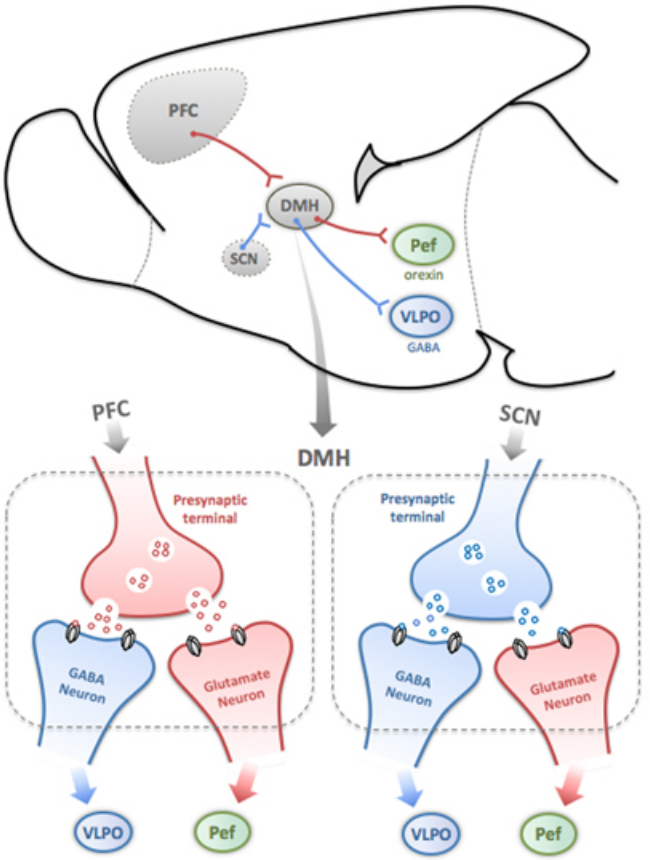

Supplemental Figure 1 Neuroanatomical illustration of the brain circuitry in relation to sleep mechanisms. Both glutamatergic and GABAergic neurons in the DMH receive direct innervation from both GABAergic neurons in the SCN and glutamatergic neurons in the prelimbic and infralimbic areas of the PFC. Then, glutamatergic DMH-Pef projection innervates excitatory orexin-containing neurons in the Pef, whereas GABAergic DMH-VLPO projection innervates inhibitory GABA-containing neurons in the VLPO.

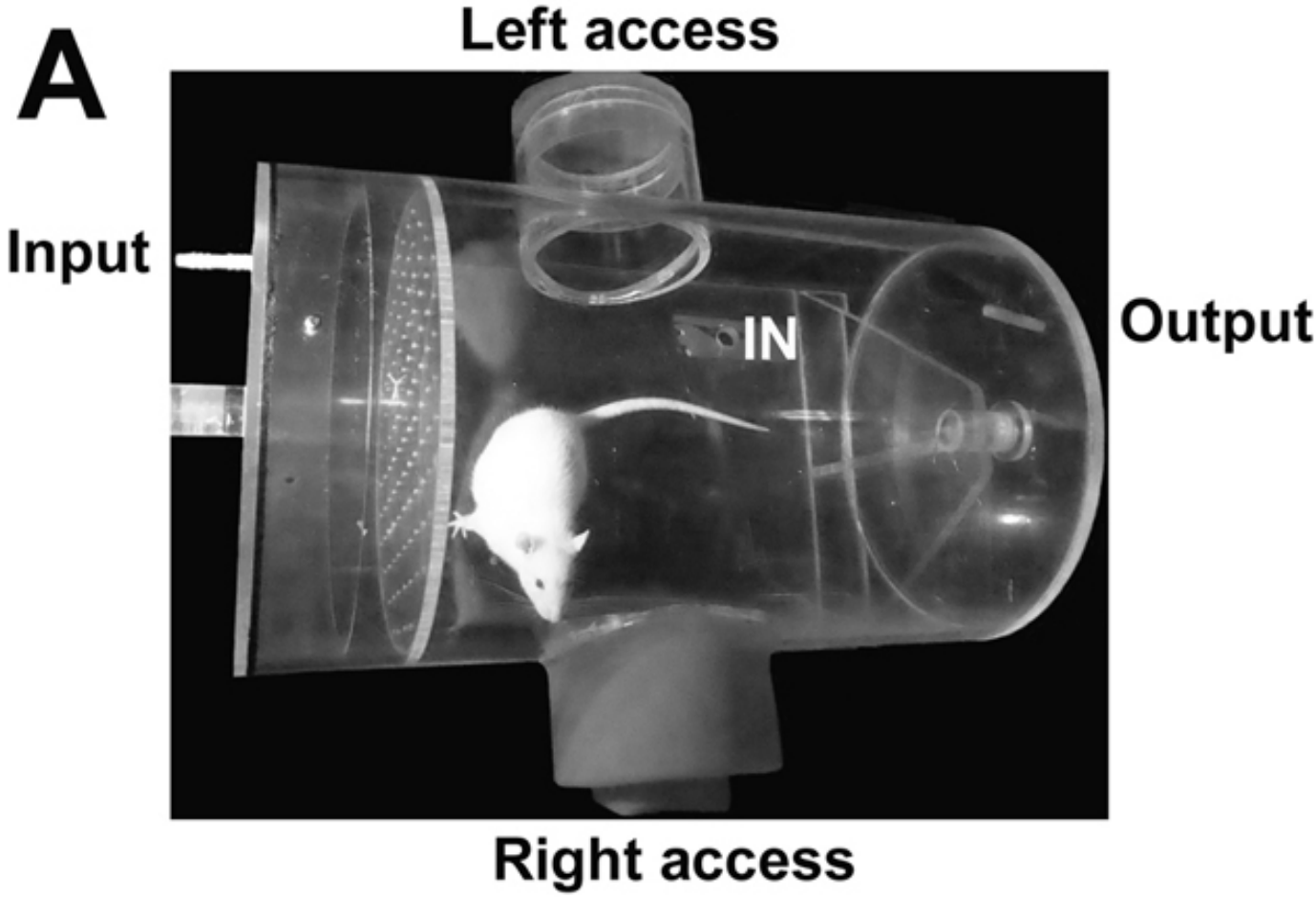

Supplemental Figure 2 The rotating anesthetic chamber for quantification of induction and recovery time. Five minutes after a rat is placed in the sealed Plexiglas chamber (length 40 cm × diameter 25 cm), a mixture of anesthetic and oxygen gas was continuously delivered into the chamber via a calibrated vaporizer and oxygen flow meter from the input hole while air inside the chamber can be pulled out through the output hole. An experimenter can access the rat with hands through the left and right access windows (diameter 11 cm) and inject the rat through the injection hole on the top (IN). See Methods for detailed procedures for the quantification of anesthesia induction and recovery times.

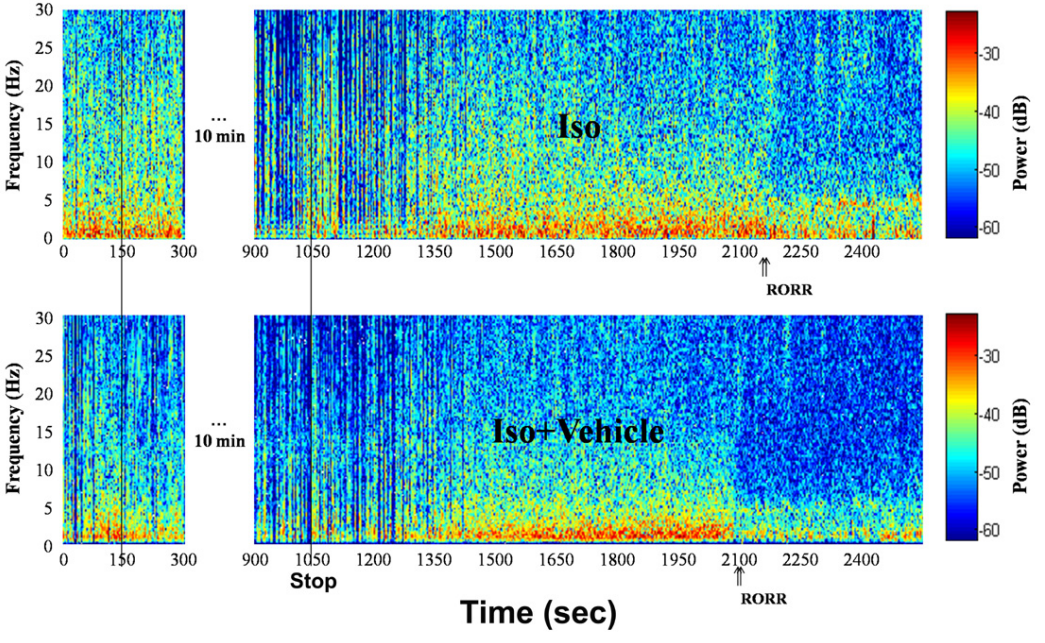

Supplemental Figure 3 EEG Spectrograms. Sample spectrograms (5 repetitions) from rats receiving isoflurane anesthesia (Iso) with or without a vehicle injection given 15 min before the end of isoflurane anesthesia (Stop). The double arrows indicate the time point when rats show RORR.

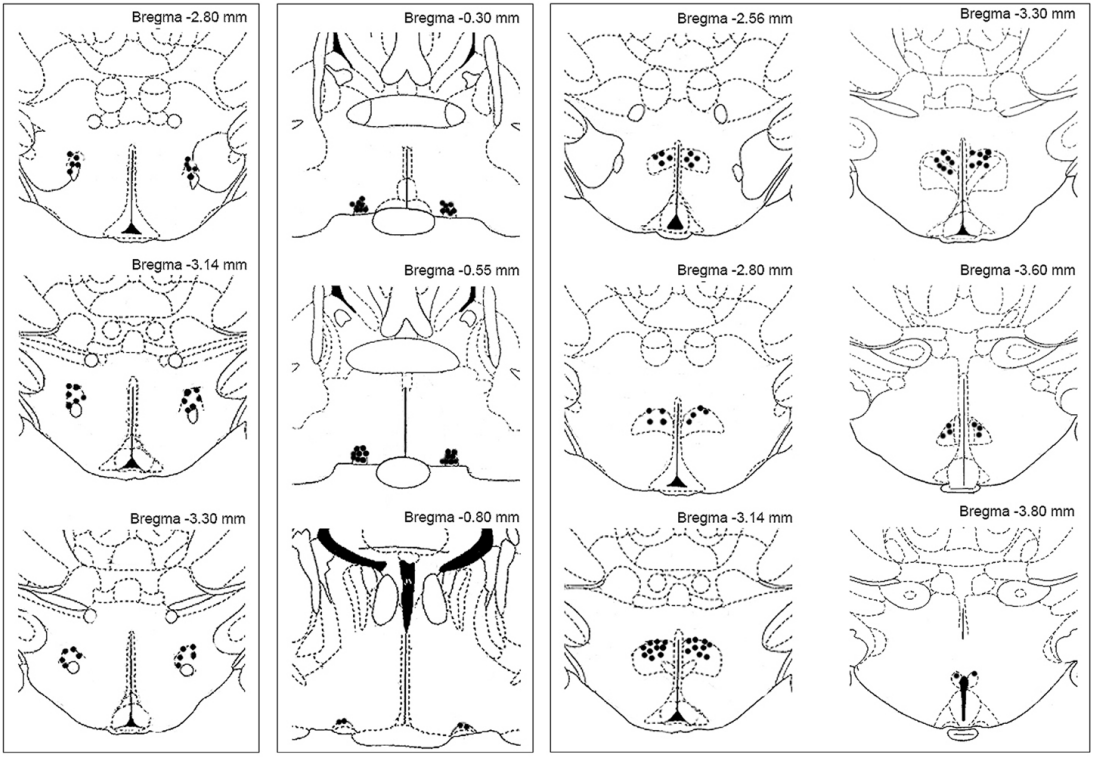

Supplemental Figure 4 Location of intra-hypothalamus injection of AM281, bicuculline or MK801. Histograms show reconstructions of histology sections illustrating intra-Pef, intra-VLPO and intra-DMH injection sites of AM281, bicuculline or MK801. Animals with injection sites outside the Pef, VLPO or DMH are excluded.

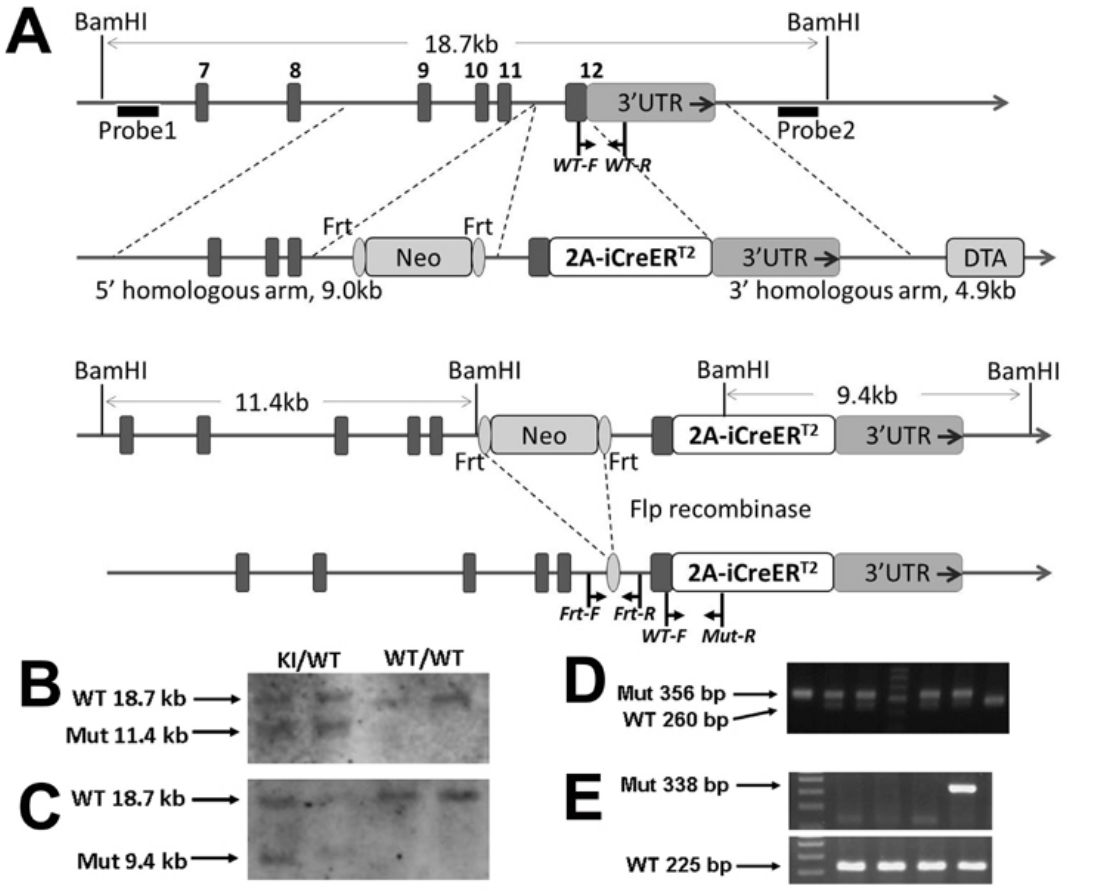

Supplemental Figure 5 Generation of vGlut2-iCreERT2 knock-in mice. (A) Targeting Strategy. The 9.0 kb fragment containing vGlut2 Exons 9, 10 and 11 and related introns is used as the 5' homologous arm. The 4.9 kb fragment involving vGlut2 3' UTR is used as the 3' homologous arm. 2A-CreERT2 is introduced between the coding sequence of vGlut2 Exon12 and 3'UTR. Neo cassette flanked by frt sites is inserted within intron11 to avoid disrupting poly(A) signal of vGlut2 and promoter region of GM7336, a gene nearby. (**B**, **C**) Representative Southern blot (3 repetitions) for selection of positive ES cell clones. Probe 1 identified an 18.7 kb wild type band and an 11.4 kb mutant band (B). Probe 2 identified an 18.7 kb wild type band and a 9.4 kb vGlut2-iCreERT2 knock-in band (C). (**D**, **E**) Representative genotyping results (> 50 repetitions) of offspring. PCR amplification using vGlut2-Frt-F plus vGlut2-Frt-R (D) or both vGlut2-WT-F plus vGlut2-WT-R and vGlut2-WT-F plus vGlut2-Mut-R (E), clearly shows the germline transmission of the vGlut2-iCreERT2 knock-in allele. KI, vGlut2-iCreERT2 knock-in; Mut, mutant; WT, wild type.

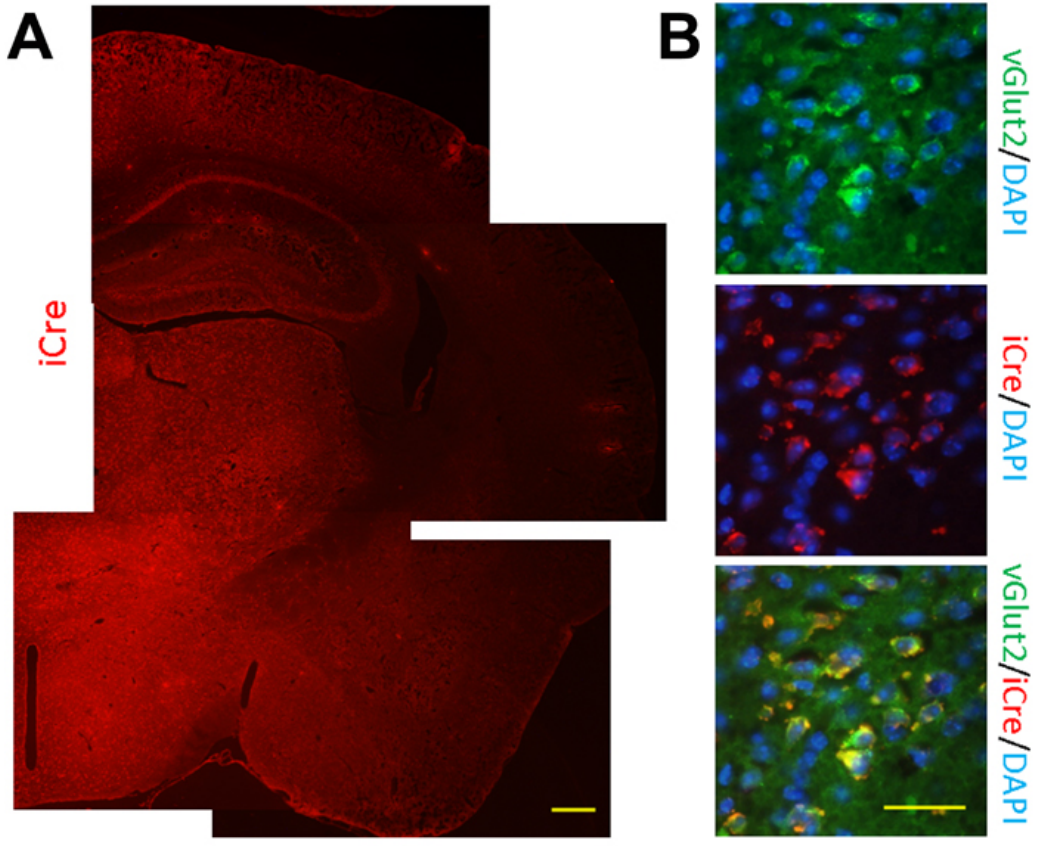

Supplemental Figure 6 Fluorescence *in situ* hybridization for iCre in vGlut2-iCreERT2 mouse brain sections. (A) Stitched images show the distribution of iCre (red) in the brain. The expression pattern of iCre tested by FISH here is consistent with previous study. Scale bar = 500 μm. (**B**) Representative images (3 repetitions) show double FISH for vGlut2 (green) and iCre (red) combined with DAPI staining (blue). The iCre is expressed in vGlut2+ cells in the DMH (yellow). Scale bar = 50 μm.

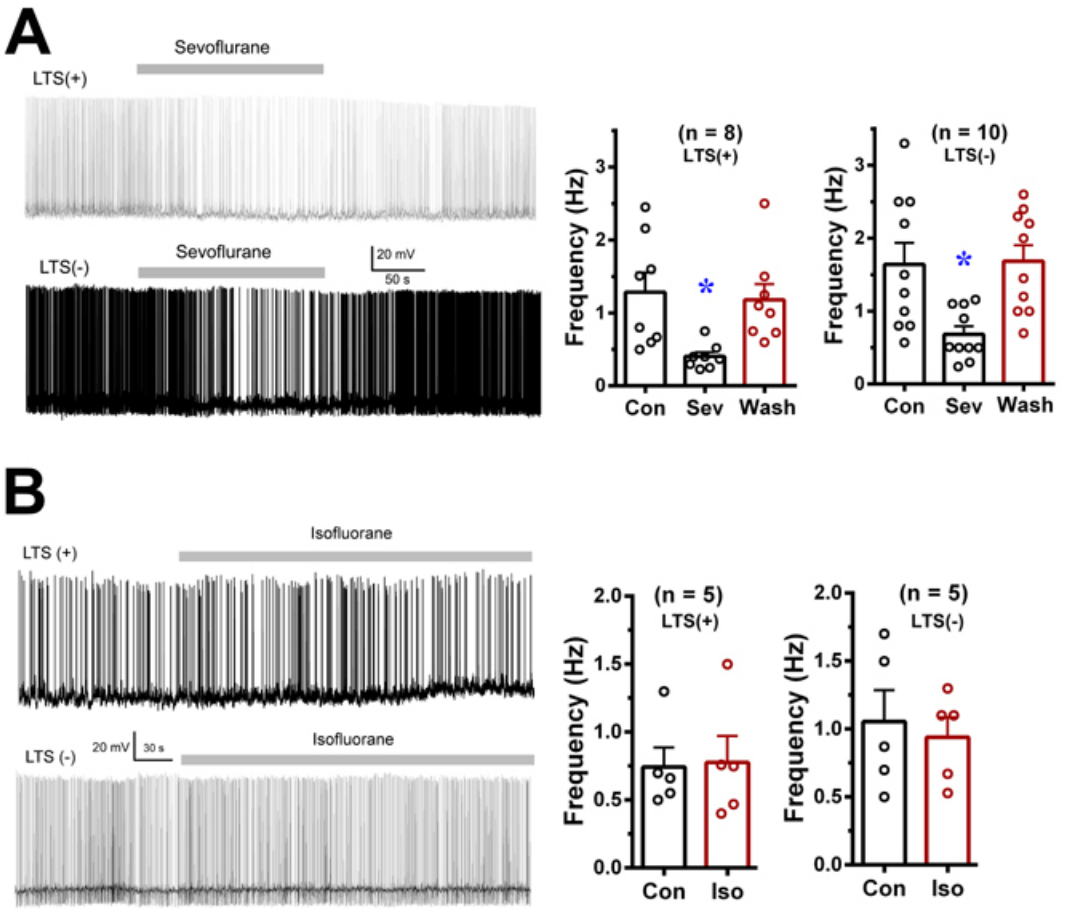

Supplemental Figure 7 Anesthetic suppression of DMH GABAergic and glutamatergic neurons. (A) The representative traces (left) and summary histograms (right) show that relative to baseline (Con), bath application of sevoflurane (Sev) induces rapid hyper-polarization of the membrane potential and significantly decreases of the firing rate of both LTS(+) and LTS(-) neurons in the DMH, which return to the baseline levels after washout (Wash). (B) The representative traces (left) and summary histograms (right) show that relative to baseline (Con), bath application of isoflurane (Iso) in the presence of AM281 does not significantly affect the membrane potential and firing rate of both LTS(+) ($p = 0.7347$) and LTS(-) neurons ($p = 0.4115$) in the DMH. All summary graphs show means ± SEMs; n = numbers of rats recorded in each group. * $p < 0.05$ vs. control, Tukey's *post-hoc* test after one-way ANOVA (A: LTS(+), $F_{2,21} = 5.759$, $p < 0.05$; LTS(-), $F_{2,27} = 6.656$, $p < 0.01$) or Student *t* test (B).

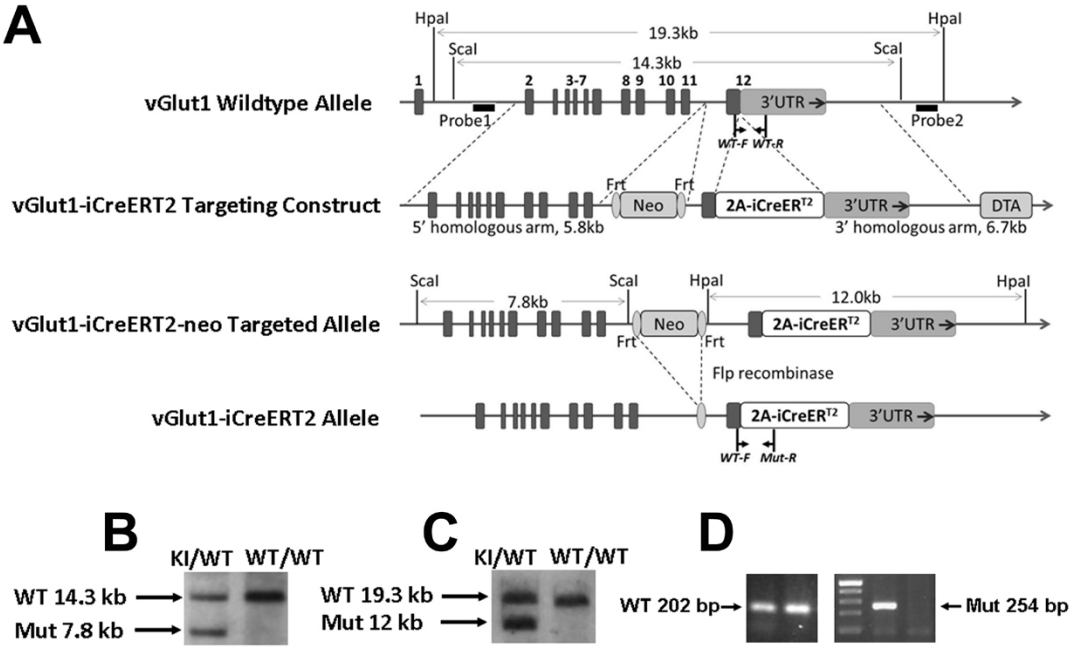

Supplemental Figure 8 Generation of vGlut1-iCreERT2 knock-in mice. (A) Targeting Strategy. The 5.8 kb fragment containing those from vGlut1 Exon 2 to Exon 11 and related introns was used as the 5' homologous arm. The 6.7 kb fragment involving vGlut1 3'UTR and downward sequence was used as the 3' homologous arm. 2A-CreERT2 was introduced between the coding sequence of vGlut1 Exon12 and 3'UTR. Neo cassette flanked by frt sites was inserted within intron11 to avoid disrupting poly(A) signal of vGlut1. (**B**, C) Representative Southern blot (3 repetitions) for selection of positive ES cell clones. Probe 1 identified a 14.3 kb wild type band and a 7.8 kb mutant band (B). Probe 2 identified a 19.3 kb wild type band and a 12 kb vGlut1-iCreERT2 knock-in band (C). (**D**) Representative genotyping results (> 50 repetitions) of offspring mice. PCR amplification using vGlut1-CreERT2-WT-F plus vGlut1-CreERT2-WT-R (lane 1), or using vGlut1-CreERT2-WT-F plus vGlut1-CreERT2-Mut-R (lane 2), clearly showed the germline transmission of the vGlut1-iCreERT2 knock-in allele. WT, wild type; KI, vGlut1-iCreERT2 knock-in; Mut, mutant.

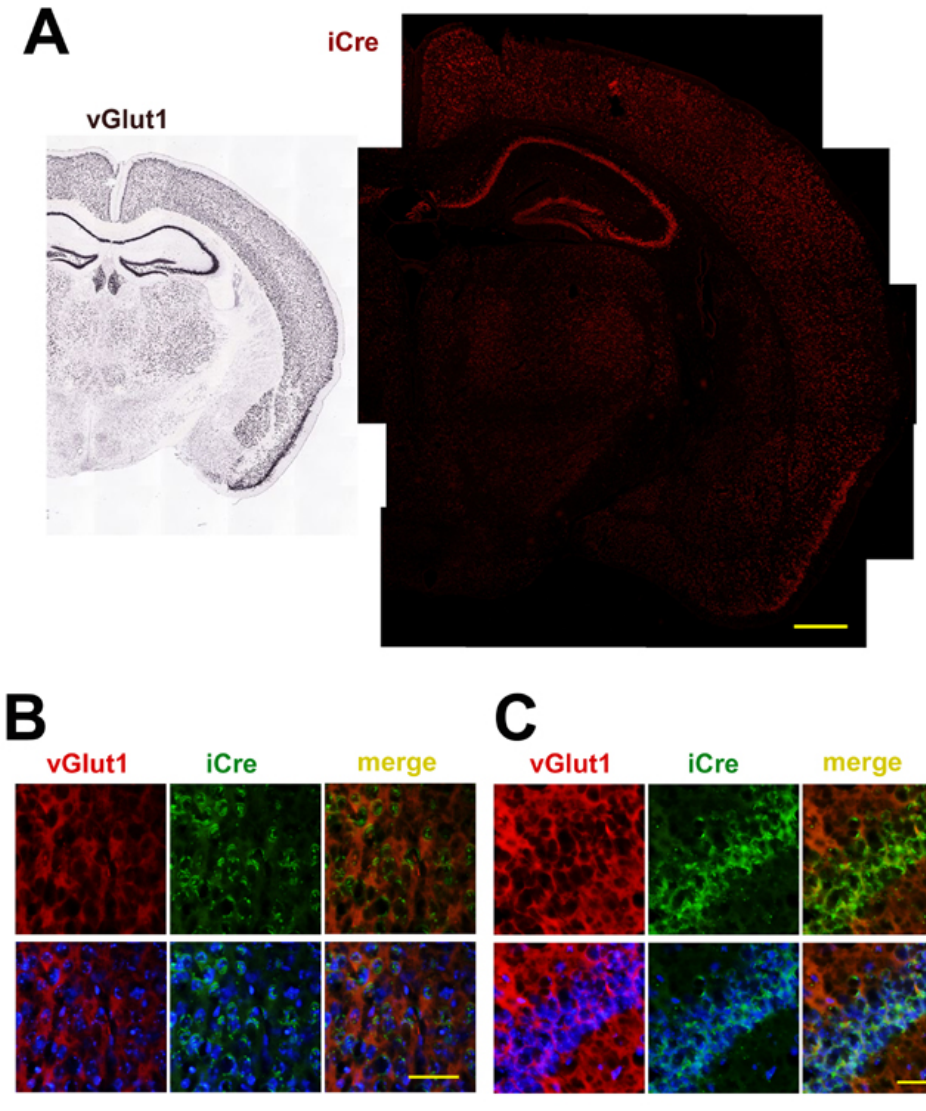

Supplemental Figure 9 Fluorescence *in situ* hybridization for iCre in vGlut1-iCreERT2 mouse brain sections. (A) Images together show the distribution of iCre (red) in the whole brain. The expression pattern of iCre tested by FISH was consistent with the expression pattern of vGlut1 which was highly expressed in the cortex and hippocampus. Scale bar = 500 μm. (**B**, C) Representative images (3 repetitions) show double FISH for vGlut1 (red) and iCre (green) combined with DAPI staining (blue). The iCre is expressed in vGlut1+ cells (yellow) in the cerebral cortex (B) and hippocampus (C). Scale bar = 50 μm.

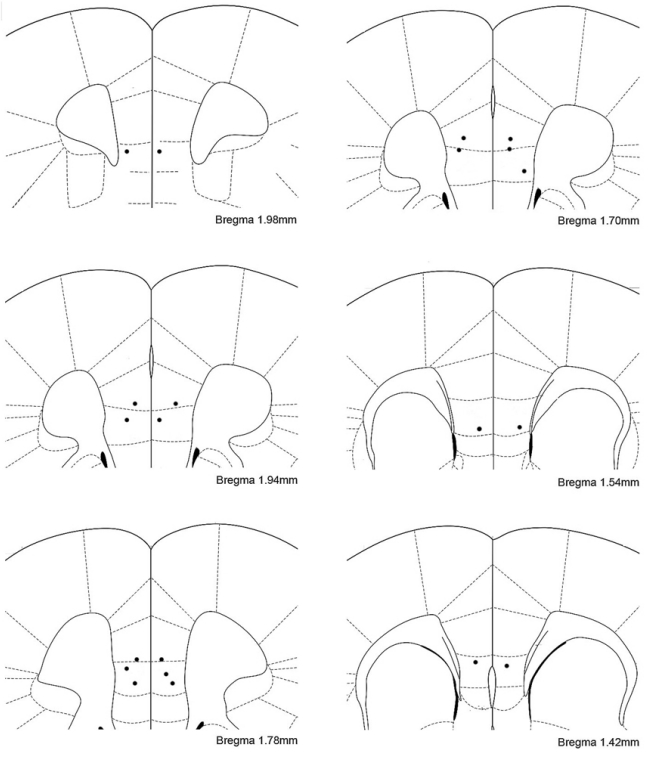

Supplemental Figure 10 Location of intra-PFC injection of AAV-Camk2-Cre. Histograms show reconstructions of histology sections illustrating AAV-Camk2-Cre injection sites in the prelimbic and infralimbic areas of the PFC. Animals with injection sites outside the prelimbic and infralimbic areas are excluded.

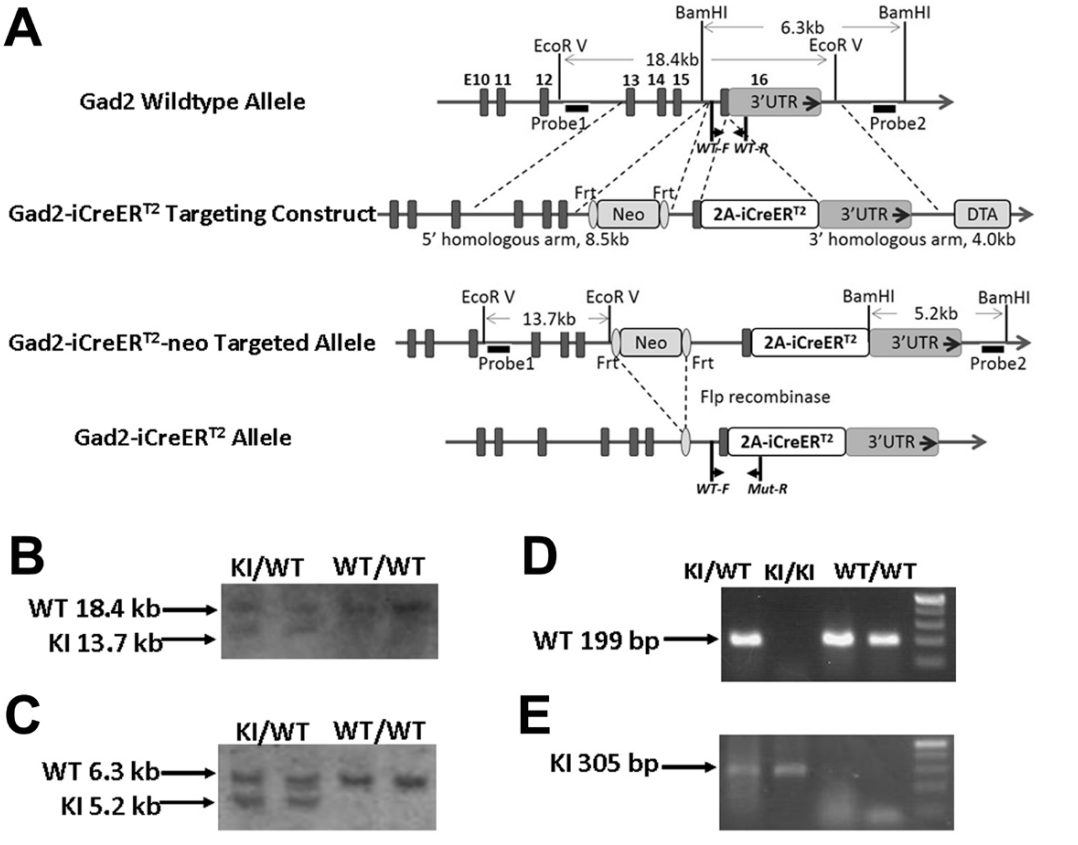

Supplemental Figure 11 Generation of GAD65-iCreERT2 knock-in mice. (A) Targeting Strategy. The 8.5 kb fragment containing Gad2 Exons 13, 14 and 15 and related introns was used as the 5' homologous arm. The 4.0 kb fragment involving Gad2 3'UTR was used as the 3' homologous arm. 2A-CreERT2 was introduced between the coding sequence of Gad2 Exon16 and 3'UTR. Neo cassette flanked by frt sites was inserted within intron15 to avoid disrupting poly(A) signal of Gad2 and promoter region of Apbb1ip, a gene nearby. (**B**, **C**) Representative Southern blot (3 repetitions) for selection of positive ES cell clones. Probe 1 identified an 18.4 kb wild type band and a 13.7 kb mutant band (B). Probe 2 identified a 6.3 kb wild type band and a 5.2 kb Gad2-iCreERT2 knock-in band (C). (**D**, **E**) Representative genotyping results (> 50 repetitions) of offspring. PCR amplification using Gad2-WT-F plus Gad2-WT-R (D), or using Gad2-WT-F plus Gad2-Mut-R (E), clearly showed the germline transmission of the Gad2-iCreERT2 knock-in allele. WT, wild type; KI, Gad2-iCreERT2 knock-in.

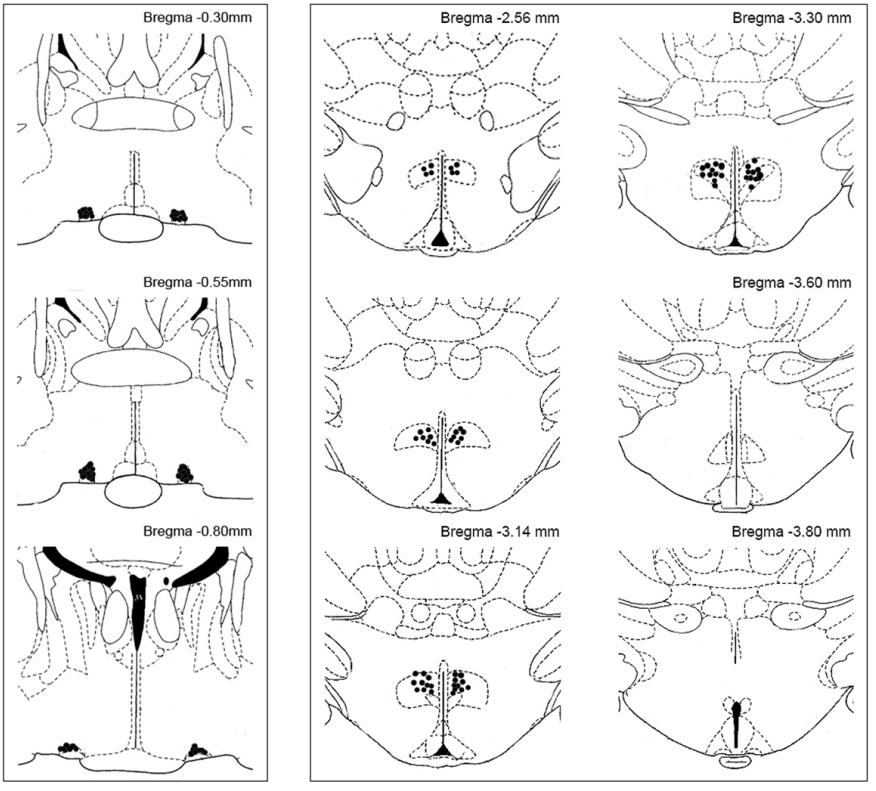

Supplemental Figure 12 Location of intra-hypothalamus injection of PRV-Cre and DREADD. Histograms show reconstructions of histology sections illustrating injection sites of intra-VLPO injection of PRV-Cre and intra-DMH injection of hM4Di or hM3Dq. Animals with injection sites outside the VLPO or DMH are excluded.

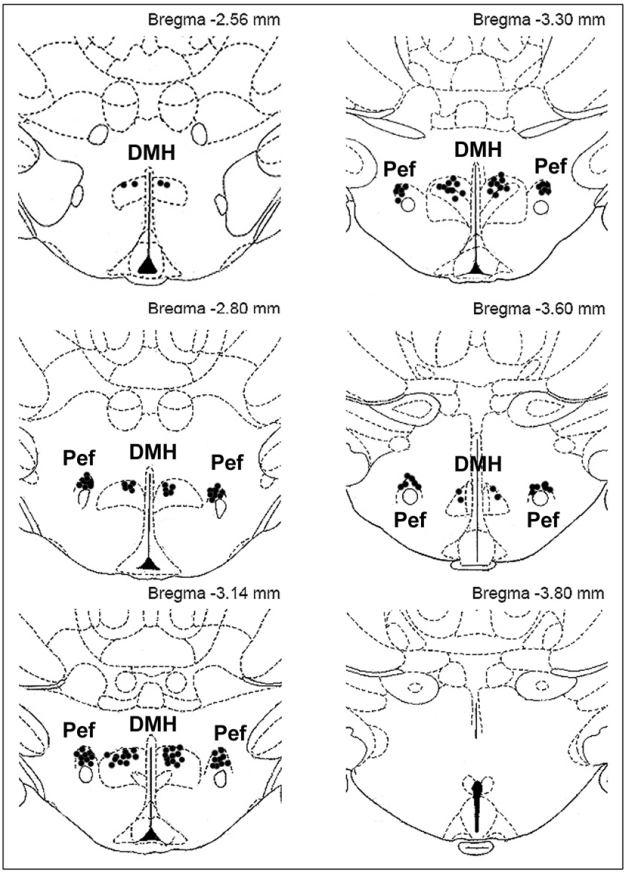

Figure S13

Supplemental Figure 13 Location of intra-hypothalamus injection of PRV-Cre and DREADD. Histograms show reconstructions of histology sections illustrating injection sites of intra-Pef injection of PRV-Cre and intra-DMH injection of hM4Di or hM3Dq. Animals with injection sites outside the Pef or DMH are excluded.

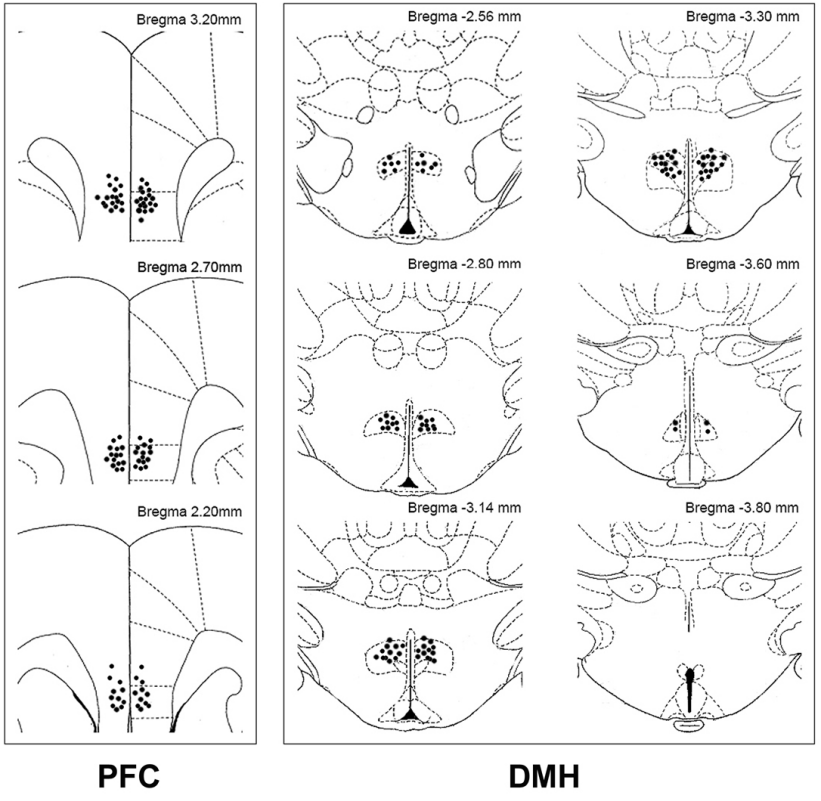

Supplemental Figure 14 Location of intra-cerebral injection of PRV-Cre and DREADD. Histograms show reconstructions of histology sections illustrating injection sites of intra-DMH injection of PRV-Cre and intra-PFC injection of hM4Di or hM3Dq. Animals with injection sites outside the DMH or PFC are excluded.

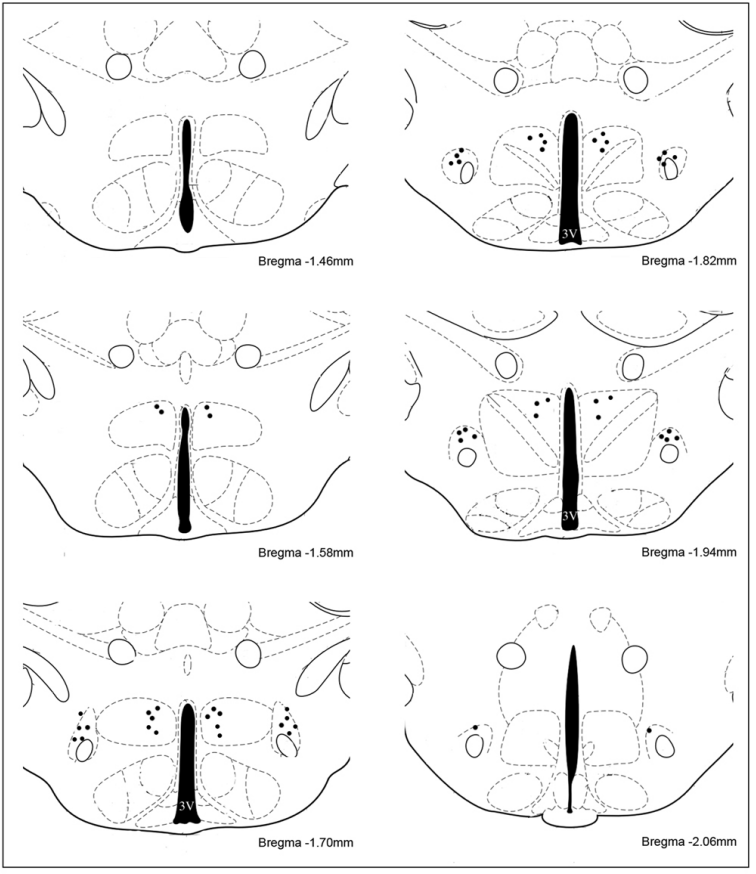

Supplemental Figure 15 Location of intra-hypothalamus injection of DREADD and CNO. Histograms show reconstructions of histology sections illustrating hM3Dq injection sites in the DMH 2 weeks before intra-Pef injection of CNO. Animals with injection sites outside the DMH or Pef are excluded.

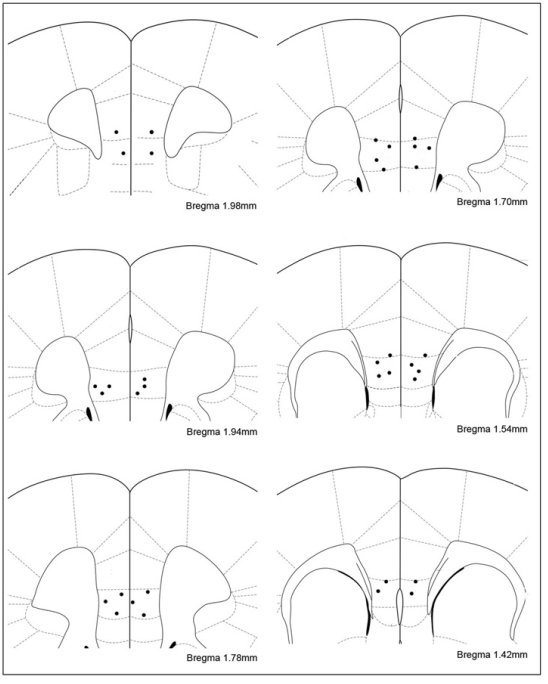

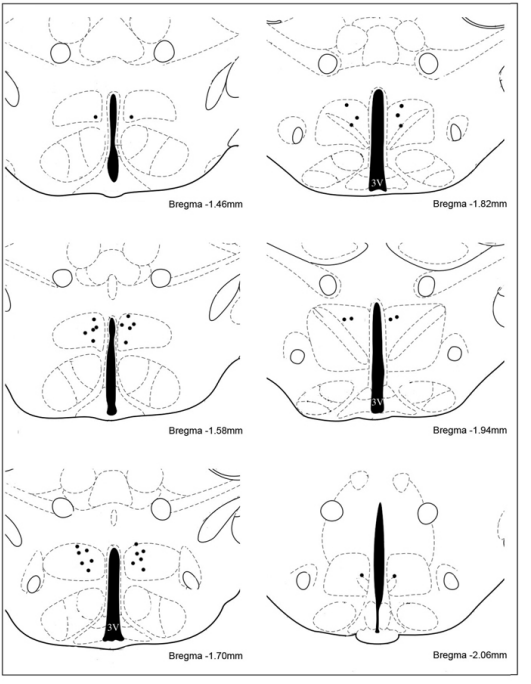

PFC **DMH**

Supplemental Figure 16 Location of intra-cerebral injection of DREADD and CNO. Histograms show reconstructions of histology sections illustrating hM3Dq injection sites in the prelimbic and infralimbic areas of the PFC 2 weeks before intra-DMH injection of CNO. Animals with injection sites outside the PFC or DMH are excluded.

Primers	Sequence	Tm (℃)	Product Size (bp)
vGlut1-iCreERT2-WT-F	CTGGCTGGCAGTGACGAAAG	59	WT: 202
vGlut1-iCreERT2-WT-R	CGCTCAGGCTAGAGGTGTATGG	60	
vGlut1-iCreERT2-WT-F	CTGGCTGGCAGTGACGAAAG	59	Mut: 254
vGlut1-iCreERT2-Mut-R	TGGTGCACAGTCAGCAGGTTG	61	
vGlut2-iCreERT2-WT-F	AGAATGGAGGCTGGCCTAACG	60	WT: 225
vGlut2-iCreERT2-WT-R	TTGAACAGCAAGACTTGCTTGG	58	
vGlut2-iCreERT2-WT-F	AGAATGGAGGCTGGCCTAACG	60	Mut: 338
vGlut2-iCreERT2-Mut-R	GCACACAGACAGGAGGATCTTC	59	
vGlut2-iCreERT2-Frt-F	GATGGTTGGTACATGCCTATCAC	57	WT: 260, Mut: 356
vGlut2-iCreERT2-Frt-R	CAAATACACCTATAGGCTGCAGAG	57	
Gad2-iCreERT2-WT-F	CTGCAGCAACTCACCAAGACA	59	WT: 199
Gad2-iCreERT2-WT-R	AACTGTACTCTACTGTGACACCAC	58	
Gad2-iCreERT2-WT-F	CTGCAGCAACTCACCAAGACA	59	Mut: 305
Gad2-iCreERT2-Mut-R	GCACACAGACAGGAGCATCTTC	59	

Supplemental Table 1 The primer sequences for identification of vGlut1, vGlut2 and Gad2 knock-in mice. WT, wild type fragment; Mut, mutant fragment; bp, base pairs.